ACS APPLIED MATERIALS & INTERFACES

RESEARCH ARTICLE

www.acsami.org

Designing Novel Hybrid Materials by One-Pot Co-condensation: From Hydrophobic Mesoporous Silica Nanoparticles to Superamphiphobic Cotton Textiles

C. Pereira,[†] C. Alves,[†] A. Monteiro,[†] C. Magén,[‡] A. M. Pereira,[§] A. Ibarra,[‡] M. R. Ibarra,[‡,⊥] P. B. Tavares,[#] J. P. Araújo,[§] G. Blanco,[||] J. M. Pintado,[||] A. P. Carvalho,[¶] J. Pires,[¶] M. F. R. Pereira,[△] and C. Freire*[,†]

[†]REQUIMTE, Departamento de Química e Bioquímica, Faculdade de Ciências, Universidade do Porto, 4169-007 Porto, Portugal

[‡]Laboratorio de Microscopías Avanzadas, Instituto de Nanociencia de Aragón and Departamento de Física de la Materia Condensada, Universidad de Zaragoza, 50018 Zaragoza, Spain

[§]IFIMUP and IN—Institute of Nanoscience and Nanotechnology, Departamento de Física e Astronomia, Faculdade de Ciências, Universidade do Porto, 4169-007 Porto, Portugal

[⊥]Instituto de Ciencia de Materiales de Aragón and Departamento de Física de la Materia Condensada, CSIC-Universidad de Zaragoza, 50009 Zaragoza, Spain

[#]Departamento de Química and CQ-VR, Universidade de Trás-os-Montes e Alto Douro, 5001-801 Vila Real, Portugal

[||]Departamento de Ciencia de Materiales e Ingeniería Metalúrgica y Química Inorgánica, Facultad de Ciencias, Universidad de Cádiz, Campus Rio San Pedro, 11510 Puerto Real, Cádiz, Spain

[¶]Departamento de Química e Bioquímica, Centro de Química e Bioquímica, Faculdade de Ciências, Universidade de Lisboa, 1749-016 Lisboa, Portugal

[△]Laboratório de Catálise e Materiais (LCM), Laboratório Associado LSRE/LCM, Departamento de Engenharia Química, Faculdade de Engenharia, Universidade do Porto, 4200-465 Porto, Portugal

Supporting Information

ABSTRACT: This work reports the synthesis and characterization of mesoporous silica nanoparticles (MSNs) functionalized with tridecafluorooctyltriethoxysilane (F13) and their in situ incorporation onto cotton textiles. The hybrid MSNs and the functional textiles were prepared by a one-pot co-condensation methodology between tetraethylorthosilicate (TEOS) and F13, with hexadecyltrimethylammonium chloride (CTAC) as the template and triethanolamine as the base. The influence of the F13 to TEOS molar ratio (1:10, 1:5 and 1:3) on the nanoparticle morphology, porosity, degree of functionalization, and hydro/oleophobic properties is discussed. The hybrid nanosilicas presented high colloidal stability and were spherical and monodispersed with average particle size of ∼45 nm. They also showed high surface areas, large pore volumes, and a wormhole-type mesoporous structure. The increase in the organosilane proportion during the co-condensation process led to a more radially branched wormhole-like mesoporosity, a decrease in the surface area, pore volume, and amount of surface silanol groups, and an enrichment of the surface with fluorocarbon moieties. These changes imparted hydrophobic and oleophobic properties to the materials, especially to that containing the highest F13 loading. Cotton textiles were coated with the F13-MSNs through an efficient and less time-consuming route. The combination between surface roughness and mesoporosity imparted by the MSNs, and the low surface energy provided by the organosilane resulted in superhydrophobic functional textiles. Moreover, the textile with the highest loading of fluorocarbon groups was superamphiphobic.

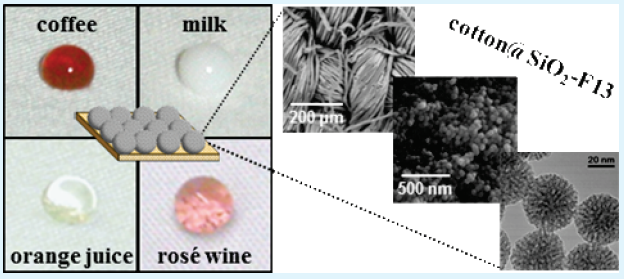

KEYWORDS: co-condensation functionalization, mesoporous silica nanoparticles, functional textiles, hydrophobicity, oleophobicity, tridecafluorooctyltriethoxysilane

1. INTRODUCTION

Since the birth of nanotechnology, new challenges emerged in various areas of research toward the design of hybrid nanomaterials and technological processes. Mesoporous silica nanoparticles (MSNs) with a MCM-41 type porous structure are a class of versatile nanomaterials with tremendous potential for a broad spectra of applications, including catalysis,[1,2] controlled drug

Received: February 20, 2011
Accepted: May 26, 2011
Published: May 26, 2011

Scheme 1. Schematic Representation (not drawn to scale) of: (a) Synthesis of F13-MSNs and (b) Fabrication of Hybrid Cotton Textiles Functionalized with F13-MSNs, by One-Pot Co-condensation Methodologies

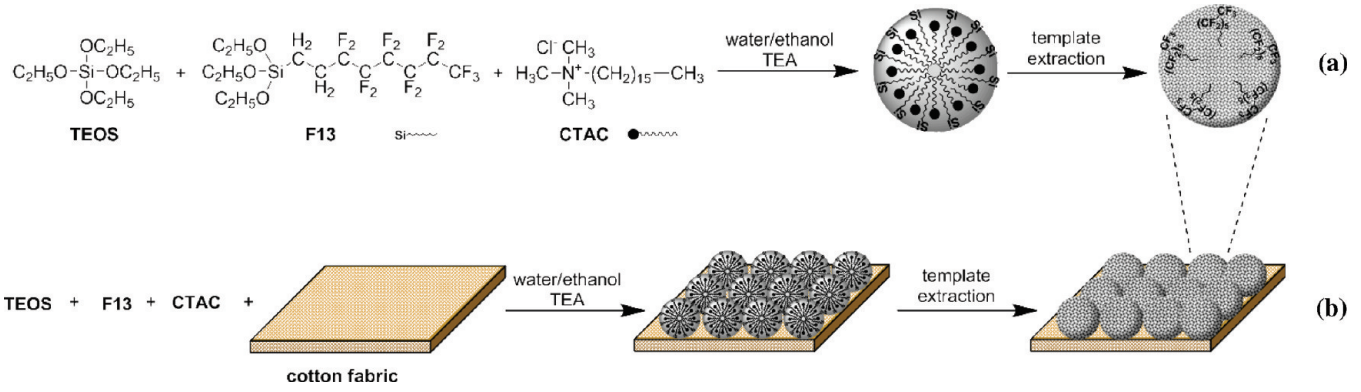

delivery,[1−3] and surface coatings.[4,5] Their high specific surface areas, ordered structure, and tunable pore sizes are some of their remarkable features. The ability to incorporate specific organic functional groups through covalent bonding is another key aspect to tailoring their properties.[2,6]

The functionalization of MSNs with organosilanes can be achieved by two main strategies: co-condensation and postgrafting. The co-condensation method is a one-step route consisting of the simultaneous condensation of a silicate precursor and one or more organosilanes, whereas the postgrafting is a two-step approach in which the organosilane is anchored to the as-synthesized silica. The co-condensation offers several advantages because it is a one-pot methodology and provides a more homogeneous distribution of the organic moieties throughout the material. Nevertheless, it may cause a decrease in the mesoscopic order and requires mild conditions for the template extraction.[1,3,7,8] Numerous research groups have been engaged in the design of co-condensation strategies to prepare organo-functionalized MSNs with high colloidal stability, high loading of functional groups and uniform particle size.[8−12] In general, the methods involved relatively high dilutions and led to particles with size higher than 100 nm. In this context, novel methodologies to reduce the particle size and tune the porosity are being pursued.

A recent breakthrough has been reported by Bein et al., who developed a novel one-pot strategy for the synthesis of MSNs with small sizes (40−150 nm), narrow particle size distributions, very high specific surface areas, and high colloidal stability.[13−15] Their method is based on the use of a polyalcohol, triethanolamine (TEA), which acts as a base, as a complexing agent for silicate precursors and as an encapsulator for mesoporous particles, thus regulating the alkoxides hydrolysis/condensation rates and limiting the particles growth and aggregation.[16,17]

Fluorocarbon-functionalized materials have been raising increased interest in a myriad of scientific and technological areas, due to the extraordinary hydro- and oleophobicity properties endowed by the fluorine-based groups.[18−20] Fluoroalkoxysilanes have been incorporated in various substrates for water/oil repellent coatings,[18,21,22] fluorophilic separations,[18,19,23] and fluorous biphasic catalysis.[18] There are a scarce number of studies regarding the incorporation of fluorocarbon groups onto mesoporous silicas by co-condensation. Mesoporous fluorinated organosilicate films and bulk mesoporous silicas have been prepared with potential use for (super)hydrophobic coatings and fluorophilic separations.[19,20,24−26] To the best of our knowledge, no report on the synthesis of hydro/oleophobic fluorinated colloidal MSNs prepared by co-condensation has been published so far.

The quest for innovative high-performance textiles has been a major milestone in the textile industry, motivated by the consumers demand for fabrics with improved properties such as (super)hydrophobicity, fire retardancy, antimicrobial properties and photochromism.[27]

The nanoscale modification of textile surfaces with silica particles emerged as a promising strategy to design materials with improved chemical and mechanical stabilities and water/oil repellence properties.[27] Recently, silica particles and hydro/oleophobic compounds have been incorporated onto textiles to fabricate superhydrophobic and (super)oleophobic textiles.[27−29] One strategy consists on the textile dip-coating either with a modified silica sol containing hydrophobic additives[30] or with a colloidal suspension of fluorocarbon-functionalized silica nanoparticles.[31] Another approach consists on the textile functionalization with silica particles formed in situ followed by an additional step of hydro/oleophobization with an epoxy-functionalized polydimethylsiloxane,[32] hexadecyltrimethoxysilane,[33,34] stearic acid[35,36] and/or with a perfluoroalkylsilane.[32,35−39] Most of these methods required long reaction times and/or multiple steps, which are major drawbacks for industrial applications. To the best of our knowledge, the one-pot functionalization of textiles with silica nanoparticles modified with hydro/oleophobic organosilanes and presenting mesoporosity, by co-condensation, has not yet been explored.

In view of these challenges, this work reports the preparation of colloidal MSNs functionalized with F13 (F13-MSNs), by one-pot co-condensation between TEOS and the organosilane, in the presence of CTAC and using TEA as base, Scheme 1a. The effect of the organosilane concentration on the nanoparticle morphology, pore structure, degree of functionalization and hydro/oleophobic properties is investigated. In the second part, cotton textiles functionalized with F13-MSNs (F13-fabrics) were fabricated by the new in situ one-step co-condensation methodology, Scheme 1b. The influence of the TEOS:F13 ratio on the textural properties and water/oil repellency of the hybrid fabrics is examined.

2. EXPERIMENTAL SECTION

2.1. Materials and Reagents. TEOS (≥99%), aqueous CTAC solution (25 wt %) and TEA (≥99.5%) were purchased from Fluka,

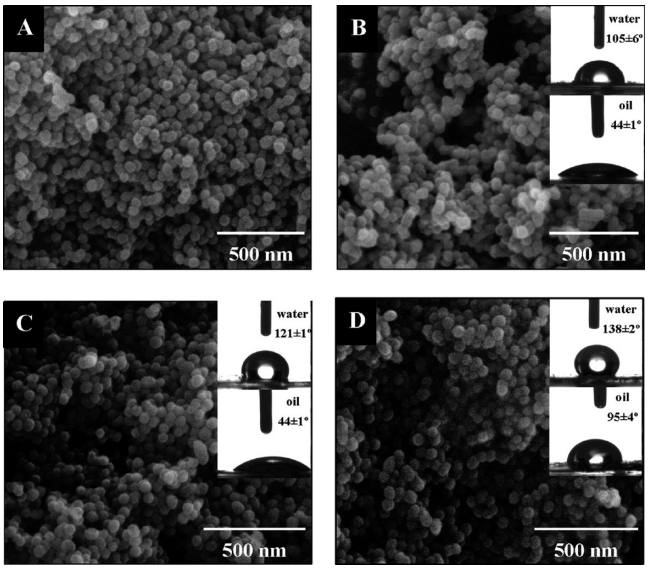

Figure 1. SEM micrographs of (A) SiO_2, (B) F13_1:10, (C) F13_1:5, and (D) F13_1:3 nanomaterials. Inset of B—D: Photographs of water and oil droplets on pellets of the F13-MSNs and CA values.

ammonium nitrate (analytical grade) was from Merck and hydrochloric acid (37%, analytical grade) was supplied by Panreac. The F13 organosilane, Dynasylan F 8261, was kindly offered by Evonik-Goldschmidt GmbH. Ethanol and toluene (analytical grade) were purchased from Merck. Ultrapure water (Millipore, specific resistivity: 18 MΩ cm) was used throughout the experiments. A 100% bleached cotton textile (120 g m^{-2}) was supplied from a local fabric store.

2.2. Fabrication of the Hybrid Materials. F13-MSNs were synthesized by co-condensation between TEOS and F13 using TEA as base and CTAC as template, following procedures adapted from literature.[15] Three different molar ratios of F13 to TEOS were used: 1:10, 1:5, and 1:3. In the case of F13:TEOS molar ratio of 1:10, a stock solution containing 64.0 cm^3 of water (3.55 mol), 10.5 cm^3 of ethanol (0.179 mol), and 10.4 cm^3 of 25 wt % CTAC solution (7.86 mmol) was stirred for 10 min at room temperature. To this solution 4.1 cm^3 of TEA (0.031 mol) were added (pH 11). Afterward, 60 cm^3 of this solution were heated to 60 °C, and then 4.35 cm^3 of TEOS (19.5 mmol) and 0.748 cm^3 of F13 (1.95 mmol) were simultaneously added under vigorous stirring. The reaction mixture was stirred at 60 °C for 2 h and then cooled to room temperature. Finally, ethanol was added and the resulting F13-MSNs were isolated by centrifugation, followed by template extraction. The final molar composition of the reagents in the reaction mixtures was 1 TEOS:x F13:0.27 CTAC:1 TEA:137 water:6.2 ethanol, where x = 0.1, 0.2, or 0.3. A molar ratio of TEOS:TEA of 1:1 was chosen to minimize the particle size.[13−15] Unfunctionalized MSNs were prepared as reference, under identical experimental conditions, without adding F13. Template removal was performed by refluxing the nanosilicas twice in 150 cm^3 of an ethanolic solution of ammonium nitrate (0.25 M) for 1 h and twice in 150 cm^3 of an ethanolic solution of hydrochloric acid (0.14 M) for 1 h. Afterward the MSNs were separated by centrifugation, washed/centrifuged with ethanol twice, and finally a part was redispersed in ethanol while the remaining was air-dried. All colloidal suspensions were stable over extended periods of time (several months). The F13-MSNs will be labeled as F13_1:10, F13_1:5, and F13_1:3, where 1:10, 1:5, and 1:3 are the molar ratios of F13:TEOS. The unfunctionalized sample will be denoted as SiO_2.

Hybrid cotton textiles were prepared using the co-condensation procedure described above, with the three F13:TEOS molar ratios. More detailed information is provided in the Supporting Information.

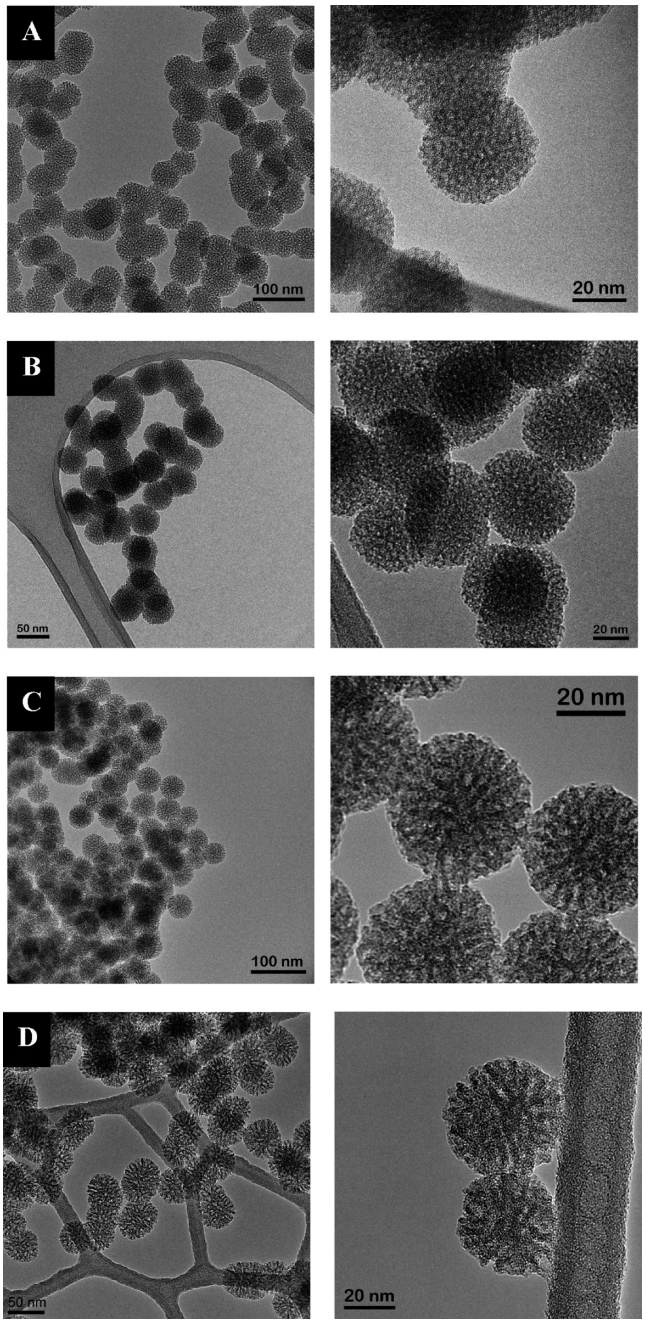

Figure 2. TEM micrographs of (A) SiO_2, (B) F13_1:10, (C) F13_1:5, and (D) F13_1:3 nanomaterials.

The functional textiles will be referred to as cot@F13_1:10, cot@F13_1:5 and cot@F13_1:3. For comparison, a square piece of cotton was functionalized with MSNs formed in situ, by adding only TEOS. This sample will be named as cot@SiO_2.

2.3. Physicochemical Characterization. Scanning electron microscopy and energy-dispersive X-ray spectroscopy were performed at Centro de Materiais da Universidade do Porto, Portugal, using a high-resolution environmental scanning electron microscope (FEI Quanta 400 FEG ESEM) equipped with an energy-dispersive X-ray spectrometer (EDAX Genesis X4M). Transmission electron microscopy images were collected in a FEI Tecnai T20 operated at 80 kV to minimize beam damage. STEM images (not shown) and X-ray microanalysis were performed in a FEI Titan operated at 80 kV and equipped

Table 1. Morphological and Textural Properties of the Mesoporous Silica-Based Nanomaterials

	particle size (nm)			textural properties				
				XRD data (nm)		N_2 adsorption−desorption isotherms data		
material	d_{SEM}[a]	d_{TEM}[b]	d_{DLS}[c]	d_{100}[d]	a_0[e]	A_{BET} ($m^2\ g^{-1}$)	V_{meso}[f] ($cm^3\ g^{-1}$)	d_{pore}[g] (nm)
SiO_2	55 ± 4	42 ± 4	116 ± 2 (0.15)	6.0	6.9	1078	0.75	3.9
F13_1:10	58 ± 3	43 ± 3	127 ± 4 (0.14)	5.0	5.7	944	0.45	3.4
F13_1:5	53 ± 5	42 ± 4	99 ± 3 (0.11)	5.5	6.4	910	0.45	3.7
F13_1:3	52 ± 3	45 ± 4	96 ± 5 (0.19)	6.0	6.9	519	0.25	4.0

[a] Average particle size estimated by SEM. [b] Average particle size estimated by TEM. [c] Average hydrodynamic diameter determined by DLS; the values between brackets correspond to the polydispersion indexes. [d] *d*-spacing corresponding to the main (100) XRD reflection: $d_{100} = \lambda / 2\text{sen}\theta$. [e] XRD unit cell parameter $a_0 = 2\, d_{100}/\sqrt{3}$, assuming an MCM-41 like hexagonal cell. [f] Mesoporous volume. [g] NLDFT pore diameter (maximum of the NLDFT pore size distribution).

with an EDAX X-ray spectrometer. Dynamic light scattering measurements were performed at 20 °C, using a Malvern Zetasizer NanoZS compact scattering spectrometer with a 4.0 mW He−Ne laser (633 nm wavelength) at a scattering angle of 170°. X-ray diffraction measurements were performed at room temperature with a Siemens D5000 diffractometer and a PW 3040/60 X'Pert Pro Röntgen diffractometer, respectively, using Cu Kα radiation (λ = 1.5406 Å) and Bragg−Brentano $\theta/2\theta$ configuration. Nitrogen adsorption−desorption isotherms at −196 °C were measured in an automatic apparatus Nova 2200e, Quantachrome. Fourier transform infrared spectra of the MSNs were collected with a Jasco FT/IR-460 Plus spectrophotometer in the range 400−4000 cm^{-1}, with 4 cm^{-1} resolution and 32 scans. The FTIR spectra of the samples after thermal treatment at different temperatures were recorded on a FTIR Bruker Vertex 70 spectrophotometer in the range 400−4000 cm^{-1}, with 4 cm^{-1} resolution and 100 scans. Attenuated total reflectance FTIR spectra of the cotton-based samples were obtained on a Perkin-Elmer Spectrum 100 spectrophotometer equipped with an ATR accessory in the range 650−4000 cm^{-1}, with 4 cm^{-1} resolution and 16 scans. Solid-state nuclear magnetic resonance spectra, ^{13}C CPMAS (cross-polarization magic angle spinning), ^{29}Si MAS, and ^{29}Si CPMAS. were recorded at Departamento de Química, Universidade de Aveiro, Portugal, on a 9.4 T Bruker Avance 400 spectrometer, at a spinning rate of 9 kHz for carbon and 5 kHz for silicon. Thermogravimetric analyses of the nanosilicas were carried out on a TA Instruments Q600 thermobalance; α-alumina was used as reference. The experiments were performed in the temperature range of 20−1000 °C, at a heating rate of 10 °C min^{-1} in He with a flow rate of 60 $cm^3\ min^{-1}$. The thermograms of the cotton-based samples were obtained on a Perkin-Elmer Pyris 1 thermobalance, under nitrogen flow (20 $cm^3\ min^{-1}$) with a heating rate of 10 °C min^{-1} between 20 and 1000 °C. Carbon and silicon elemental analyses (EA) were performed at Laboratório de Análises do Instituto Superior Técnico, Portugal. The X-ray photoelectron spectroscopy measurements were performed in a Kratos Axis Ultra DLD spectrometer equipped with monochromatic Al Kα radiation (1486.6 eV), with the X-ray source being operated at 150 W. Hydrophobicity and oleophobicity tests were performed at CITEVE, Vila Nova de Famalicão, Portugal, with a contact angle apparatus Dataphysics Contact Angle System OCA. More detailed information is described in the Supporting Information.

3. RESULTS AND DISCUSSION

3.1. Characterization of F13-MSNs. The SEM and TEM images show that all the nanomaterials are composed of quasi-spherical nanoparticles, with a wormhole-type mesoporous structure and particle size below 50 nm with narrow size

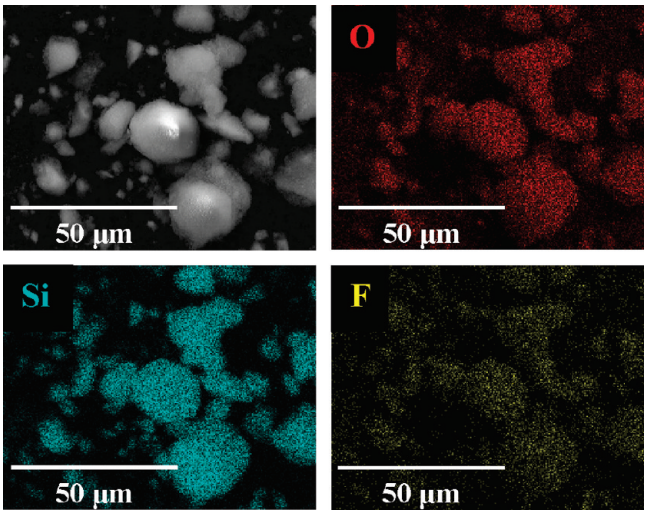

Figure 3. Low-magnification SEM image of F13_1:10 nanomaterial and corresponding X-ray maps of oxygen, silicon, and fluorine.

distributions (Figures 1 and 2, Table 1, and Figure S1 in the Supporting Information). In all samples, a high degree of monodispersion was achieved.

All the F13-MSNs present comparable average particle size, being practically independent of the F13:TEOS molar ratio. The shape and porous structure remain practically unchanged, suggesting that the incorporation of F13 does not affect the MSNs morphological and structural features; nevertheless, a slightly more disordered structure (radially branched) is observed in the case of F13_1:5 and F13_1:3. This fact is in accordance with literature, which states that the incorporation of high loadings of functional groups onto silica by co-condensation may lead to less-ordered pore arrangements.[8,19,40,41]

The preservation of the almost-spherical shape and nanosize independently of the F13 loading is also noteworthy. In literature it has been reported that the incorporation of organic groups by co-condensation may induce changes in the particles shape and porosity, when using NaOH as base, water as solvent and by changing the organosilane type or its concentration.[8,9,11] Furthermore, the synthesis of F13-functionalized mesoporous silicas by co-condensation between F13 and TEOS, in 1:4 molar ratio, using CTAB, NH_3, and water, resulted in particles with an

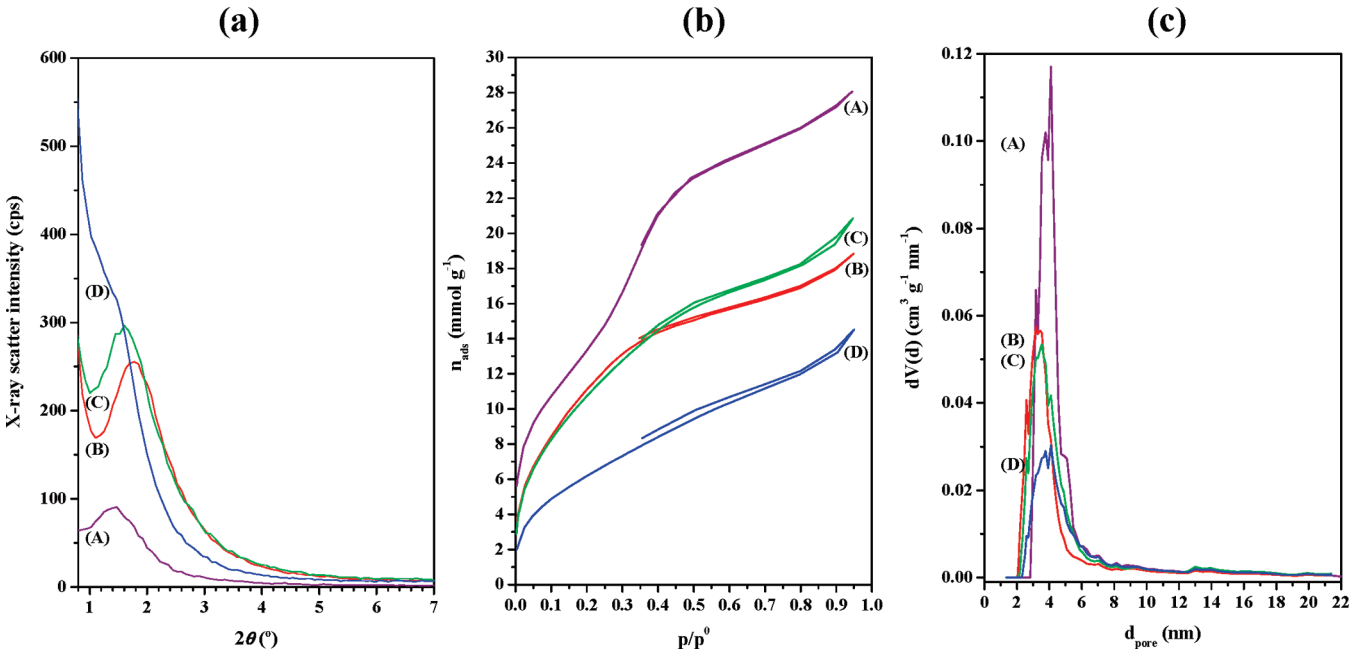

Figure 4. (a) Low-angle powder X-ray diffractograms, (b) N_2 adsorption−desorption isotherms at −196 °C, and (c) NLDFT pores size distributions of (A) SiO_2, (B) F13_1:10, (C) F13_1:5, and (D) F13_1:3 nanomaterials.

irregular morphology, micrometer size, and 2D hexagonal pore structure.[19,20] These facts suggest that ethanol and TEA have a preponderant role on tuning the particles morphology and minimizing the particles size. Bein et al. were able to change the morphology of thiol-functionalized MSNs by replacing NaOH by TEA.[14]

The EDS spectra from SEM and TEM confirm the incorporation of F13 (see Figures S2 and S3 in the Supporting Information) with the C/Si and F/Si atomic ratios increasing with the increment of F13:TEOS. The X-ray elemental maps (Figure 3 for F13_1:10) reveal that O, Si, and F are homogeneously distributed throughout the F13-MSNs.

DLS confirmed that all samples present excellent colloidal stability and corroborates the particle size trend observed by SEM and TEM (Table 1). Nevertheless, the average hydrodynamic diameters are always higher than the discrete particle sizes estimated by electron microscopy techniques.[13−15,42]

The low-angle XRD patterns show a single broad peak in the range of 1.5−1.8° 2θ, which can be attributed to the (100) Bragg reflection, assuming a MCM-41-like hexagonal structure (Figure 4a). Comparing with the XRD pattern of bulk MCM-41, which features a sharp (100) reflection peak around 2.2−2.5° 2θ and two or three additional Bragg reflections, in these nanomaterials there are no resolved peaks at higher reflections and the (100) reflection is broader and shifted toward lower 2θ values. These observations confirm the disordered wormhole-like mesoporous structure observed by TEM, as well as a deviation in the pores packing relative to MCM-41; the nanosize of the silica particles is also responsible for the peak broadening.[13,43] The diffractograms also demonstrate that the mesoporous frameworks are preserved, regardless of the quantity of incorporated F13. However, as the F13:TEOS ratio increases, the (100) reflection is progressively shifted toward lower 2θ, leading to an increase of the *d*-spacing and of the respective unit cell parameter a_0 (estimated parameter assuming a MCM-41-like hexagonal structure) (Figure 4a and Table 1). Consequently, there is a progressive increase in the pore-to-pore distance, probably due to an increase in the pore size and/or pore wall thickness.

The nanomaterials exhibit type IV isotherms, which are characteristic of mesoporous materials (Figure 4b). The specific surface areas and pore volumes of the F13-MSNs decrease in the order of F13_1:10 > F13_1:5 > F13_1:3 (Figure 4b,c and Table 1). Both F13_1:10 and F13_1:5 present very similar isotherms and textural parameters, suggesting that the increase of the F13:TEOS ratio from 1:10 to 1:5 does not induce significant changes on the material porosity. The pore size distributions show an increase in the pore diameter ongoing from F13_1:10 to F13_1:3, and a slight broadening ascribed to a small increase of the structure disorder in accordance with XRD and TEM. The pore enlargement differs from the tendency reported in literature for other mesoporous silicas functionalized by co-condensation.[7,40] However, in those studies organosilanes with short alkyl chains were incorporated. Consequently, the increase of the pore size is probably related to the long hydrophobic chains of F13 and to the interactions between F13, TEOS, and CTAC during the co-condensation reaction.

FTIR spectroscopy confirmed the complete removal of the template through the absence of the characteristic bands of CTAC in the spectra of the extracted SiO_2 and F13 MSNs (more details in the Supporting Information).[13,19,43,44] The FTIR spectra of the F13-MSNs (Figure 5a and Figure S4a in the Supporting Information) besides displaying the characteristic bands of the silica framework, are characterized by the appearance of several peaks which match well the fingerprint vibrational modes of the pure F13: C−H stretching (2985−2850 cm^{-1}), C−H/C−C bending (1420−1100 cm^{-1}), C−F stretching (1420−1100 cm^{-1}) and C−F deformation (1420−1100 cm^{-1} and 810−535 cm^{-1} respectively) vibrations of CH_2, CF_2 and CF_3 groups.[19,45−47] Upon the increase of the F13:TEOS ratio, it is noteworthy a gradual reduction on the intensity of the OH stretching and bending vibration bands and of the band from the

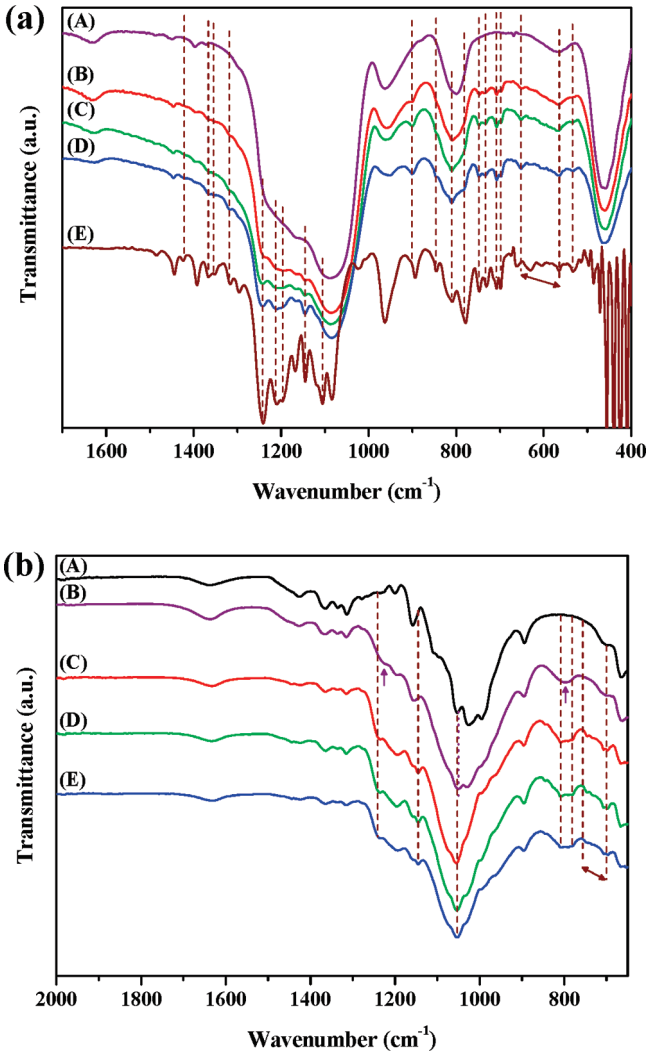

Figure 5. (a) FTIR spectra of (A) SiO_2, (B) F13_1:10, (C) F13_1:5, (D) F13_1:3, and (E) F13 in the 1700−400 cm^{-1} region. (b) FTIR-ATR spectra of (A) cotton, (B) cot@SiO_2, (C) cot@F13_1:10, (D) cot@F13_1:5, (E) cot@F13_1:3, and (F) F13 in the 2000−650 cm^{-1} region. The arrows and dotted lines highlight the characteristic peaks of silica and F13, respectively.

Si−OH stretching vibrations (~960 cm^{-1}), anticipating an increase in the nanomaterial's hydrophobicity.

The ^{29}Si MAS and CPMAS NMR spectra of all MSNs (Figure 6a,b present peaks at −111 and −102 ppm, which correspond to Q^4 and Q^3 resonances, respectively, and are associated to the fully condensed silica units and to silica with one terminal silanol group; the weak Q^2 shoulder around −95 ppm indicates that the geminal silanol groups are almost absent in all samples.[8,14,15,20] In the F13-MSNs two additional peaks are detected around −67 and −59 ppm which are respectively associated to T^3 and T^2 silicon environments, revealing the anchorage of F13 through 3- and 2-fold covalent grafting.[8,14,15,20]

The relative concentrations of the Q^n and T^m sites determined by deconvolution of the ^{29}Si MAS NMR spectra are summarized in Table 2. In all the materials a high degree of silica condensation was achieved and the degree of F13 incorporation (based on $(T^3 + T^2)/(Q^4 + Q^3 + Q^2 + T^3 + T^2)$) increases ongoing from F13_1:10 to F13_1:3. Furthermore, the relative intensity of T^3 is higher than that of T^2, indicating that most of F13 moieties are highly cross-linked to the nanoparticle walls.[8,14,15] The increase on the F13:TEOS ratio leads to a gradual decrease of the $(Q^3 + Q^2)/Q^4$ ratio, pointing out to a reduction on the amount of surface silanols relative to the siloxane units, in accordance with FTIR.

The ^{13}C CPMAS NMR spectra of the F13-MSNs (Figure 6c, for F13_1:3) exhibit the characteristic chemical shifts of F13.[48] The absence of the characteristic resonance peaks of CTAC also proved the complete extraction of the template.[8,49] The peaks at 15 and 59 ppm are due to the presence of ethoxy groups generated by the incomplete hydrolysis of F13.[40,50]

The amount of fluorocarbon groups incorporated in the hybrid nanomaterials was quantified by EA, TGA and XPS; the theoretical carbon and F13 contents were also estimated from the amount of TEOS and F13 in the starting reaction mixture and considering the T^2 and T^3 percentages determined by NMR (Table 3).

EA results for the F13-MSNs show that the C/Si ratio increases in the order F13_1:10 < F13_1:5 < F13_1:3, confirming, quantitatively, the increase in the organosilane loading as the concentration of F13 raised; moreover, very high F13 functionalization efficiencies were achieved (>94%) for all the F13:TEOS ratios.

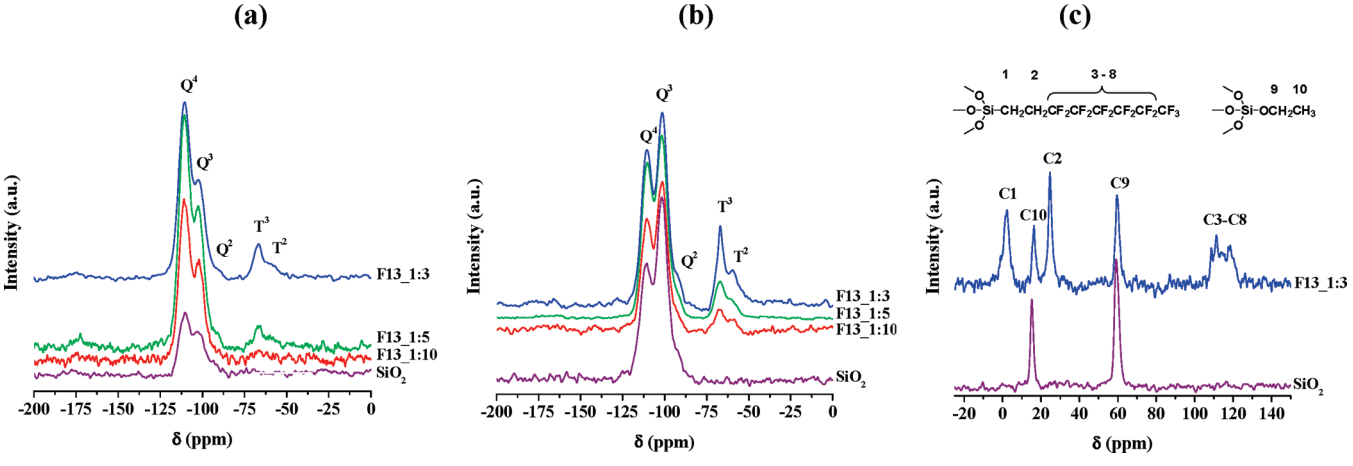

Figure 6. (a) ^{29}Si MAS, (b) ^{29}Si CPMAS, and ^{13}C CPMAS NMR spectra of the MSNs and bands assignments.

Table 2. ^{29}Si Chemical Shifts and Relative Concentrations of Q^n and T^m Resonances Obtained by Curve Deconvolution of the ^{29}Si MAS NMR Spectra of the Mesoporous Silica-Based Nanomaterials

	Q^4		Q^3		Q^2		T^3		T^2		
material	δ (ppm)	%	δ (ppm)	%	δ (ppm)	%	δ (ppm)	%	δ (ppm)	%	$(T^3+T^2)/(T^3+T^2+Q^4+Q^3+Q^2)$ (%)
SiO_2	−111	52	−102	35	−94	13					
F13_1:10	−111	60	−102	27	−96	8	−67[a]	3[a]	−59[a]	2[a]	5[a]
F13_1:5	−111	60	−102	28	−95	6	−67	4	−59	2	6
F13_1:3	−111	59	−102	24	−96	6	−67	8	−59	3	11

[a] Estimated value due to the low intensity of the peaks associated with a low level of organic functionalization.

Table 3. Carbon, Silicon, and Organic Contents of the Mesoporous Silica-Based Nanomaterials Predicted Theoretically and Determined by EA and TGA

	theoretical content[a]				EA content				TGA content[b]			
material	F13 (%)	F13 (mmol g^{-1})	C (%)	C (mmol g^{-1})	Si (%)	Si (mmol g^{-1})	C (%)	C (mmol g^{-1})	weight loss[c] (%)	F13[d] (mmol g^{-1})	C (%)	C (mmol g^{-1})
SiO_2					40	14.2	5.1	4.2	10.5			
F13_1:10	32.0	0.74	7.7	6.39	29	10.3	9.6	8.0	28.1	0.79	8.2	6.81
F13_1:5	48.4	1.12	11.6	9.65	28	10.0	11.1	9.2	34.2	0.96	9.9	8.28
F13_1:3	61.0	1.41	14.5	12.11	23	8.2	13.7	11.4	46.1	1.30	13.4	11.12

[a] Calculated from the composition of TEOS and F13 in the starting reaction mixture and considering T^3 and T^2 ratio, see text. [b] TGA under He atmosphere. [c] Partial weight loss in the temperature range of 200−600 °C (SiO_2) or 300−650 °C (F13-MNPs). [d] F13 loading calculated considering T^3 and T^2 ratio, see text.

All the TGA curves (see Figure S5 in the Supporting Information) display an initial weight loss until ∼130 °C due to the removal of physisorbed water and ethanol from the porous structure.[20,50] In the F13-MSNs, a significant weight loss is observed between 300 and 650 °C, which is associated to the decomposition of the fluorocarbon chains[19,20,24,25] as confirmed by FTIR at different temperatures (see Figure S6 in the Supporting Information). The F13 loadings, estimated from the weight loss in that temperature range, increase in the order F13_1:10 < F13_1:5 < F13_1:3 (Table 3). Nevertheless, in all cases, the carbon contents determined by TGA are lower than those obtained by EA, because of trace amounts of ethanol or base in the samples that are desorbed below 200 °C.

The surface atomic percentages and core-level binding energies (BEs) of the different elements determined by XPS are summarized in Table 4 and Table S1 in the Supporting Information.

In all samples, the absence of nitrogen and chlorine also confirmed the efficient template extraction. For F13-MSNs the F/Si and C/Si ratios increase in the order of F13_1:10 < F13_1:5 < F13_1:3. The appearance of a strong band in the F 1s spectra around 687.8−688.4 eV and of several new bands in the C 1s spectra related to C−H/C−C (284.6 eV), C−O/$-CF_2-\underline{C}H_2-$ (286.0−286.2 eV), $-\underline{C}F_2-CH_2-$ (288.1−288.3 eV), $-CF_2-CF_2-$ (290.8−291.1) and $\underline{C}F_3-CF_2-$ (293.2−293.5 eV) groups certify the incorporation of fluoroalkyl chains (Table S1 and Figure S7 in the Supporting Information).[21,51,52] It is noteworthy that the percentage content associated with the C 1s components from CF_2 and CF_3 groups increases from F13_1:10 (∼46%) to F13_1:3 (∼62%). In all the F13-MNPs, the carbon surface loading (XPS) is higher than the bulk one (EA), evidencing that the organosilane is preferentially immobilized onto the MSNs external surface. Finally, the O 1s spectra, besides exhibiting the characteristic peak of pure silica at 531.1−532.4 eV, present a shoulder at higher BEs associated with unhydrolyzed ethoxy groups from the F13 precursor.

Table 4. Surface Atomic Percentages for Silica- and Cotton-Based Materials Obtained by XPS[a]

	atomic %			
material	C 1s	O 1s	F 1s	Si 2p
SiO_2	10.0	62.0		28.0
F13_1:10	18.0	43.7	18.0	20.3
F13_1:5	19.0	41.4	19.7	19.9
F13_1:3	22.7	30.6	31.3	15.4
cotton	66.7	33.3	–	–
cot@SiO_2	4.8	66.1	–	29.1
cot@F13_1:10	25.3	34.5	25.9	14.3
cot@F13_1:5	25.5	30.2	31.4	12.9
cot@F13_1:3	28.4	32.7	27.1	11.8

[a] Determined by the areas of the respective peaks in the high-resolution XPS spectra.

3.2. Hydrophobicity and Oleophobicity Properties of F13-MSNs. In the insets of Figure 1 are illustrated representative photographs of water and oil droplets on the surface of the nanomaterials pellets and the corresponding contact angles (CAs). In the SiO_2 sample, the water and oil droplets are almost immediately absorbed, demonstrating that the surface is amphiphilic. In contrast, the F13-MSNs are hydrophobic, with the water CA gradually increasing with the F13 loading and reaching 138° in the case of F13_1:3, a value very close to the superhydrophobic behavior (CA > 150°). These values are higher than

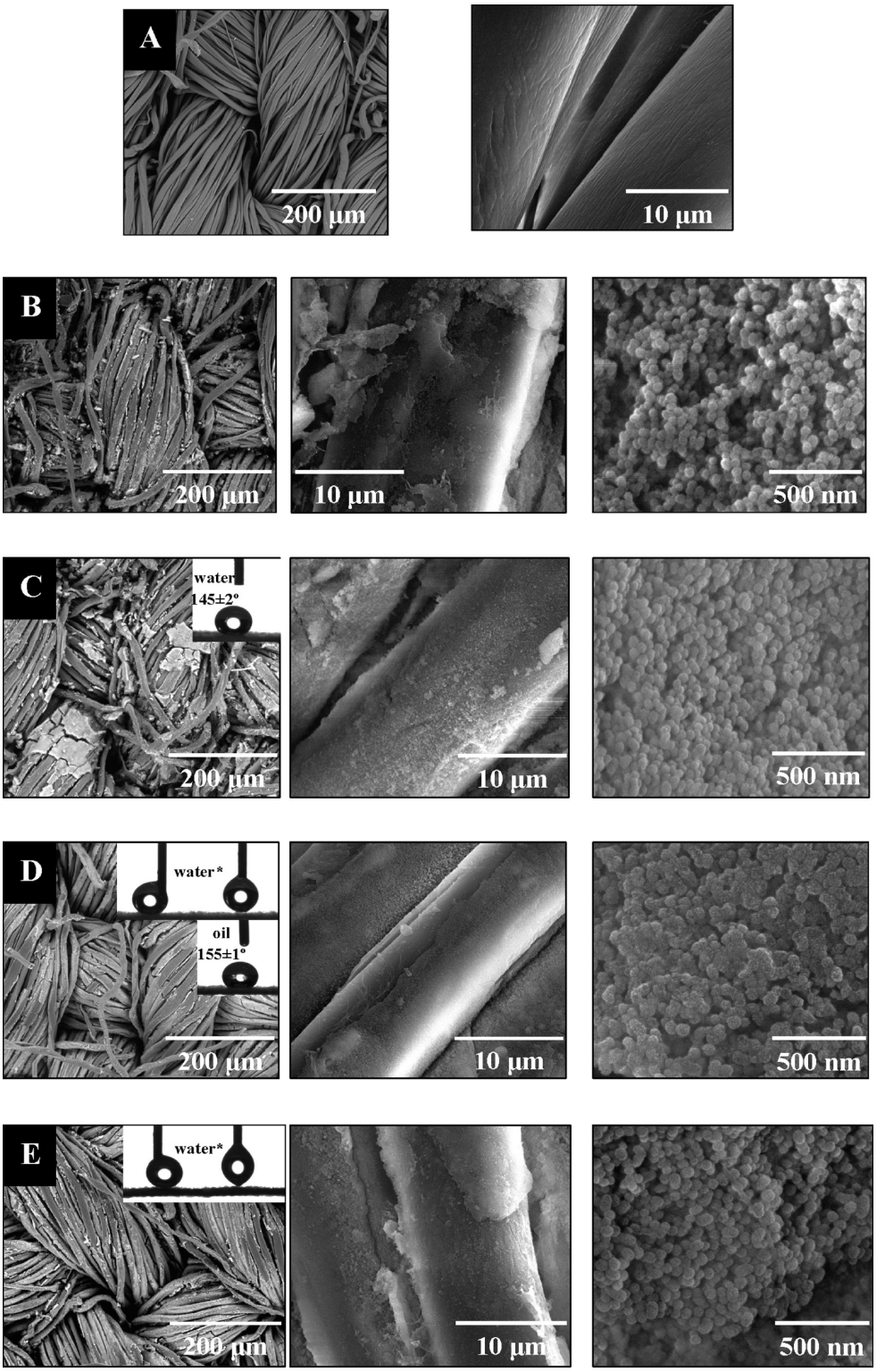

* Not possible to determine, see video clip in Supporting Information.

Figure 7. SEM micrographs with different magnifications of (A) cotton, (B) cot@SiO_2, (C) cot@F13_1:10, (D) cot@F13_1:5, and (E) cot@F13_1:3. Inset of C−E: Photographs of water and oil droplets on the surface of the hybrid fabrics and CA values. Note: the images of the superhydrophobic cot@F13_1:5 and cot@F13_1:3 samples are taken from video clips.

those reported for mesoporous fluorinated organosilicate films (CAs up to 108°),[24] highlighting the potentialities of these novel MSNs. The oil CAs increase from 44 to 95°, so the MSNs with the highest F13 loading are oleophobic. On the other hand, for the other two F13-based samples, although the oil CAs are very similar, the oil absorption rate decreases from F13_1:10 to

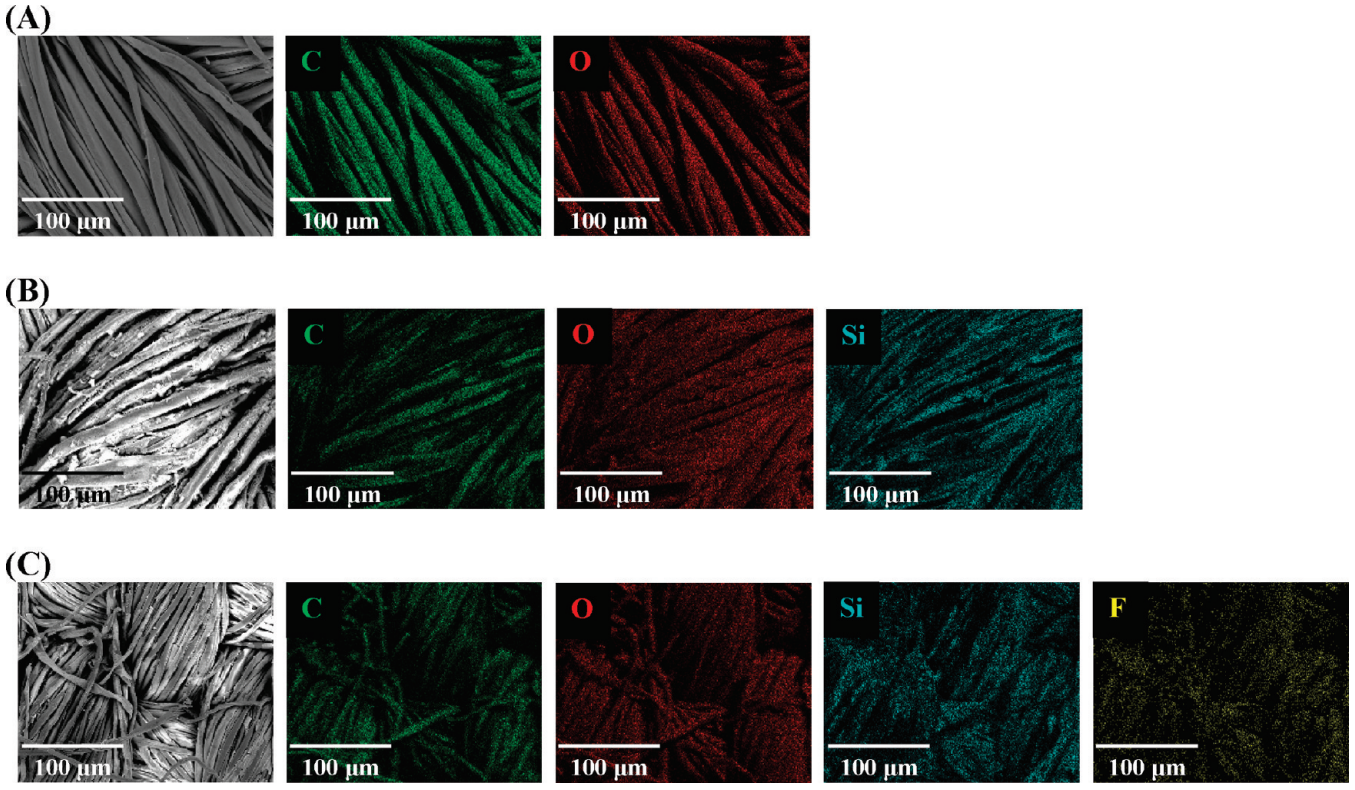

Figure 8. Low-magnification SEM image of (A) cotton, (B) cot@SiO_2, and (C) cot@F13_1:5 textiles, and corresponding X-ray maps.

F13_1:5. These trends are directly related to the surface chemical composition of the nanomaterials, in particular with: (i) the gradual decrease of the amount of silanol groups and physisorbed water on the nanomaterials surface and, more importantly, (ii) the progressive enrichment of the surface with CF_2 and CF_3 groups, which are the functional entities that confer hydrophobicity and oleophobicity properties to the materials.[24,52] The nanomaterials porous structure namely the increase of pore sizes and the reduction of the surface areas and pore volumes as the F13 concentration increases may also contribute to the observed CAs (roughness effect).

In view of these results, these F13-MSNs are potential candidates for the development of hydro/oleophobic surfaces. Consequently, in the second part of this work, we prepared functional cotton textiles modified with F13-MSNs through the in situ one-pot co-condensation methodology, Scheme 1b, and investigated their water and oil repellency properties.

3.3. Fabrication of Functional Textiles. The SEM images of the pristine cotton (Figure 7) show its smooth longitudinal fibril structure. The high-magnification micrographs of the functional textiles (Figure 7) reveal that the cotton fibers are coated with tiny silica nanospheres with the same morphology and average particle size as the bare MSNs, imparting nanoscale surface roughness. In cot@SiO_2 and cot@F13_1:10 the nanoparticles do not fully cover the fiber surface but, with the increase of the F13 concentration, they seem to be more uniformly distributed throughout the textile surface, leading to a more compact coating.

The EDS spectra (see Figure S8 in the Supporting Information) confirm the existence of Si and F in the F13-fabrics, indicating the successful grafting of the nanoparticles; the fluorine content is almost similar in all samples, being slightly higher in cot@F13_1:5. The X-ray elemental maps (Figure 8) confirm that these elements are homogeneously distributed throughout the fabrics surface.

The original cotton presents a diffractogram typical of cellulose with a monoclinic crystal symmetry with space group $P2_1$, see Figure S9 in the Supporting Information. From the Le Bail refinement, the unit-cell parameters were estimated as a = 7.607 Å, b = 10.7441 Å, c = 8.1274 Å, and β = 87.49°, in accordance with literature.[53,54] The presence of silica in the functional textiles is visualized by the decrease of the characteristic peaks of cotton (002), (101) and (110;011) due to the superimposition with the (111) broad peak from the amorphous silica (at $2\theta \approx 22.4°$).[55] Taking into account the quantity of silica phase, the amount of nanomaterial incorporated in the hybrid fabrics is in the range of 21−31%. The low-angles diffractograms of the F13-fabrics (see Figure S10 in the Supporting Information) exhibit a shoulder at $2\theta \approx 2°$, which is absent in the diffractogram of the pristine cotton, and points out to the existence of porosity from the grafted MSNs.

The FTIR-ATR spectrum of the uncoated cotton (Figure 5b and Figure S4b in the Supporting Information) displays the characteristic bands of cellulose.[45,56] In the spectra of the F13-fabrics (Figure 5b and Figure S4b in the Supporting Information), new peaks are detected at 1241, 1145, 808, and 781 cm^{-1} and in the 745−700 cm^{-1} range and the cotton bands in the 1140−914 cm^{-1} region become broader, with the peak around 1053 cm^{-1} being even more perceptible, sustaining the incorporation of the F13-MSNs on the fabric.[31,45,47] Furthermore, a significant reduction of the OH stretching band around 3315 cm^{-1} is observed.

The thermogravimetric curves of all samples (see Figure S11 in the Supporting Information) exhibit an initial weight loss

below 100 °C due to the removal of physisorbed water and residual solvent. The total weight loss decreases in the order cotton (93.84%) > cot@F13_1:3 (92.81%) > cot@F13_1:5 (90.99%) > cot@F13_1:10 (88.95%) > cot@SiO_2 (87.40%). In the F13-fabrics, the major weight loss occurs between 300 and 650 °C, similarly to the F13-MSNs, and decreases in the order cot@F13_1:3 (81.07%) ~ cot@F13_1:5 (81.02%) > cot@F13_1:10 (80.73%). These features confirm that cot@SiO_2 and cot@F13_1:10 contain the highest fractions of inorganic component, whereas cot@F13_1:5 and cot@F13_1:3 contain the highest loadings of organosilane, in accordance with SEM-EDS.

XPS results of cotton-based samples are summarized in Table 4 and Table S2 in the Supporting Information. In the F13-fabrics, besides carbon and oxygen, fluorine and silicon are also detected. Furthermore, no chlorine or nitrogen was detected, indicating the efficient surfactant removal. The C 1s spectra (see Table S2 and Figure S7 in the Supporting Information) present the five components detected in the spectra of the F13-MSNs: see section 3.1. The bands observed in the F 1s (see Figure S7 in the Supporting Information), O 1s and Si 2p regions are also characteristic of F13 and silica. Nevertheless, their BEs are generically higher than those of the corresponding MSNs, suggesting the covalent immobilization of the nanoparticles onto cotton.[31] The carbon surface content increases in the order cot@SiO_2 < cot@F13_1:10 < cot@F13_1:5 < cot@F13_1:3, whereas the silicon one decreases in the same order. Among the F13-fabrics, cot@F13_1:5 contains the highest fluorine surface loading and the highest contribution from the C 1s components of the CF_2 and CF_3 groups. This suggests that the surface of this material is more enriched in fluorocarbon groups and that the additional increase of the F13:TEOS ratio to 1:3 does not provide additional advantages in terms of textiles topology, particle distribution, degree of MSN incorporation, and F13 loading.

3.4. Hydrophobicity and Oleophobicity Properties of Functional Textiles. The water and oil surface repellency of the cotton-based samples was evaluated (insets of Figure 7). Because cotton has protruding fibers that stick out from the surface and present some elasticity leading to forces on the droplets, the accurate measurement of advancing and receding CAs is difficult, and so only static CAs are reported in this work.[34−37]

The cotton and cot@SiO_2 samples are amphiphilic resulting on the immediate absorption of the water and oil droplets.[31,32,39] In contrast, the surface hydrophobicity of the F13-fabrics is remarkably enhanced: cot@F13_1:10 is almost superhydrophobic exhibiting a water CA of 145°, whereas the 1:5 and 1:3 counterparts are superhydrophobic. In these two samples, it was impossible to measure the water CA, because the water droplets did not deposit on the fabrics surfaces and were always stuck to the needle (see video clips in the Supporting Information), suggesting that the adhesion force between the fabric surface and the droplet is lower than that between the needle and the droplet.[32,35,36] These superhydrophobic properties are similar to those of other cotton fabrics functionalized with silica particles and fluoroalkylsilanes prepared by different methodologies (CAs typically in the range of 134−174°).[30−32,35−39]

The cot@F13_1:5 sample is superoleophobic with an oil CA of 155°. All the other fabrics are oleophilic, although those functionalized with F13 present lower oil absorption rates than cotton and cot@SiO_2. Among all samples, cot@F13_1:5 contains the highest fluorine loading and enrichment of the surface in CF_2 and CF_3 groups, which may be responsible for the superoleophobicity properties. The oil CA of this sample is comparable to that of other superoleophobic textiles reported in literature (CAs in the range of 119−153°).[32,37,38] Therefore, the 1:5 F13:TEOS ratio seems to be the optimum ratio to fabricate functional textiles with superamphiphobic characteristics.

The remarkable performance of the novel textiles is a result of the synergy between two factors: an increase of the nanoscale surface roughness imparted by the mesoporous nanometer size silica particles combined with a significant reduction of the surface free energy due to the presence of a high concentration of fluoroalkylsilane moieties on the materials surface, which are well-known for their hydro- and oleophobic features.

4. CONCLUSIONS

The one-pot co-condensation methodology reported in this work allowed the fabrication of novel functional hybrid materials through a simple, efficient and less time-consuming route.

Hybrid F13-MSNs with average particle size of 45 nm, wormhole-type structure and high porosity were successful synthesized. These nanosilicas presented hydrophobic properties and the one with the highest F13 loading was almost superhydrophobic and oleophobic. These features were related to the progressive enrichment of the MSNs surface with fluoroalkyl moieties and consequent decrease of the amount of surface silanol groups and physisorbed water.

Novel superhydrophobic cotton textiles functionalized with F13-MSNs were fabricated through the in situ methodology. The enhanced surface roughness imparted by the MSNs and the reduction of the surface free energy induced by the hydro/oleophobic F13 groups were responsible for the water repellence properties. In particular, the fabric containing the highest F13 loading was superamphiphobic. The methodology developed in this work to generate superhydrophobic and superoleophobic fabrics presents several advantages over those reported in literature and can be extended to other substrates, because it leads to the functionalization of the textile with MSNs and fluorine-based groups in a single step.

We envision that the scope of application of these organic−inorganic nanoparticles can be extended to the design of other high-performance multifunctional composites.

■ ASSOCIATED CONTENT

Supporting Information. Experimental details, core-level BEs of MSNs and textiles determined by XPS, particle size distribution histograms, EDS spectra, FTIR spectra, TGA curves, deconvoluted XPS spectra in the C 1s and F 1s core-level regions, and X-ray diffractograms of the hybrid materials (PDF); video clips of the hydrophobicity tests for cot@F13_1:5 and cot@F13_1:3 (AVI). This material is available free of charge via the Internet at http://pubs.acs.org.

■ AUTHOR INFORMATION

Corresponding Author

*Tel: +351 220402590. Fax: +351 220402659. E-mail: acfreire@fc.up.pt.

■ ACKNOWLEDGMENT

This work was funded by FCT and FEDER in the framework of Program COMPETE through Project Ref PTDC/CTM/108820/2008 and by the Portuguese-Spanish Bilateral Cooperation through Projects REF E-72/10 (Portugal) and PT2009-0126 (Spain). The authors thank Evonik-Goldschmidt GmbH for offering the organosilane and CeNTI and CITEVE (Vila Nova de Famalicão, Portugal) for assistance in TGA and CA measurements of cotton-based samples. C.P., C.A., A.M., and A.M.P. thank FCT for their grants. C.M. acknowledges the funding support from Fundación Agencia Aragonesa para la Investigación y el Desarrollo (ARAID).

■ REFERENCES

(1) Slowing, I. I.; Vivero-Escoto, J. L.; Trewyn, B. G.; Lin, V. S.-Y. *J. Mater. Chem.* **2010**, *20*, 7924.
(2) Wang, Y.; Price, A. D.; Caruso, F. *J. Mater. Chem.* **2009**, *19*, 6451.
(3) Trewyn, B. G.; Slowing, I. I.; Giri, S.; Chen, H.-T.; Lin, V. S.-Y. *Acc. Chem. Res.* **2007**, *40*, 846.
(4) Hoshikawa, Y.; Yabe, H.; Nomura, A.; Yamaki, T.; Shimojima, A.; Okubo, T. *Chem. Mater.* **2010**, *22*, 12.
(5) Pagliaro, M.; Ciriminna, R.; Palmisano, G. *J. Mater. Chem.* **2009**, *19*, 3116.
(6) Piao, Y.; Burns, A.; Kim, J.; Wiesner, U.; Hyeon, T. *Adv. Funct. Mater.* **2008**, *18*, 3745.
(7) Hoffmann, F.; Cornelius, M.; Morell, J.; Fröba, M. *Angew. Chem., Int. Ed.* **2006**, *45*, 3216.
(8) Huh, S.; Wiench, J. W.; Yoo, J.-C.; Pruski, M.; Lin, V. S.-Y. *Chem. Mater.* **2003**, *15*, 4247.
(9) Sadasivan, S.; Khushalani, D.; Mann, S. *J. Mater. Chem.* **2003**, *13*, 1023.
(10) Chen, H.-T.; Huh, S.; Wiench, J. W.; Pruski, M.; Lin, V. S.-Y. *J. Am. Chem. Soc.* **2005**, *127*, 13305.
(11) Wang, S.-G.; Wu, C.-W.; Chen, K.; Lin, V. S.-Y. *Chem. Asian J.* **2009**, *4*, 658.
(12) Gu, J.; Fan, W.; Shimojima, A.; Okubo, T. *Small* **2007**, *3*, 1740.
(13) Möller, K.; Kobler, J.; Bein, T. *Adv. Funct. Mater.* **2007**, *17*, 605.
(14) Möller, K.; Kobler, J.; Bein, T. *J. Mater. Chem.* **2007**, *17*, 624.
(15) Kobler, J.; Möller, K.; Bein, T. *ACS Nano* **2008**, *2*, 791.
(16) Verkade, J. G. *Acc. Chem. Res.* **1993**, *26*, 483.
(17) Cabrera, S.; Haskouri, J. E.; Guillem, C.; Latorre, J.; Beltrán-Porter, A.; Beltrán-Porter, D.; Marcos, M. D.; Amorós, P. *Solid State Sci.* **2000**, *2*, 405.
(18) Pagliaro, M.; Ciriminna, R. *J. Mater. Chem.* **2005**, *15*, 4981.
(19) Osei-Prempeh, G.; Lehmler, H.-J.; Rankin, S. E.; Knutson, B. L. *Ind. Eng. Chem. Res.* **2008**, *47*, 530.
(20) Osei-Prempeh, G.; Lehmler, H.-J.; Miller, A.-F.; Knutson, B. L.; Rankin, S. E. *Microporous Mesoporous Mater.* **2010**, *129*, 189.
(21) Lai, Y.; Lin, C.; Huang, J.; Zhuang, H.; Sun, L.; Nguyen, T. *Langmuir* **2008**, *24*, 3867.
(22) Hozumi, A.; McCarthy, T. J. *Langmuir* **2010**, *26*, 2567.
(23) Wang, D.; Oleschuk, R. D.; Horton, J. H. *Langmuir* **2008**, *24*, 1080.
(24) Jung, J.-I.; Bae, J. Y.; Bae, B.-S. *J . Mater. Chem.* **2004**, *14*, 1988.
(25) Bae, J. Y.; Jung, J.-I.; Seo, S.-J.; Bae, B.-S. *Microporous Mesoporous Mater.* **2007**, *98*, 283.
(26) Porcherie, O.; Guari, Y.; Reyé, C. *New J. Chem.* **2005**, *29*, 538.
(27) Mahltig, B.; Haufe, H.; Böttcher, H. *J. Mater. Chem.* **2005**, *15*, 4385.
(28) Li, X.-M.; Reinhoudt, D.; Crego-Calama, M. *Chem. Soc. Rev.* **2007**, *36*, 1350.
(29) Roach, P.; Shirtcliffe, N. J.; Newton, M. I. *Soft Matter* **2008**, *4*, 224.
(30) Mahltig, B.; Fischer, A. *J. Polym. Sci., Polym. Phys.* **2010**, *48*, 1562 and refs 13 and 24 cited therein.
(31) Wang, H.; Fang, J.; Cheng, T.; Ding, J.; Qu, L.; Dai, L.; Wang, X.; Lin, T. *Chem. Commun.* **2008**, 877.
(32) Hoefnagels, H. F.; Wu, D.; de With, G.; Ming, W. *Langmuir* **2007**, *23*, 13158.
(33) Li, Z.; Xing, Y.; Dai, J. *Appl. Surf. Sci.* **2008**, *254*, 2131.
(34) Gao, Q.; Zhu, Q.; Guo, Y.; Yang, C. Q. *Ind. Eng. Chem. Res.* **2009**, *48*, 9797.
(35) Xue, C.-H.; Jia, S.-T.; Zhang, J.; Tian, L.-Q.; Chen, H.-Z.; Wang, M. *Sci. Technol. Adv. Mater.* **2008**, *9*, 035008.
(36) Xue, C.-H.; Jia, S.-T.; Zhang, J.; Tian, L.-Q. *Thin Solid Films* **2009**, *517*, 4593.
(37) Leng, B.; Shao, Z.; de With, G.; Ming, W. *Langmuir* **2009**, *25*, 2456.
(38) Yu, M.; Gu, G.; Meng, W.-D.; Qing, F.-L. *Appl. Surf. Sci.* **2007**, *253*, 3669.
(39) Zhao, Y.; Tang, Y.; Wang, X.; Lin, T. *Appl. Surf. Sci.* **2010**, *256*, 6736.
(40) Walcarius, A.; Delacôte, C. *Chem. Mater.* **2003**, *15*, 4181.
(41) Nakamura, T.; Yamada, Y.; Yano, K. *J. Mater. Chem.* **2007**, *17*, 3726.
(42) Urata, C.; Aoyama, Y.; Tonegawa, A.; Yamauchi, Y.; Kuroda, K. *Chem. Commun.* **2009**, 5094.
(43) Qiao, Z.-A.; Zhang, L.; Guo, M.; Liu, Y.; Huo, Q. *Chem. Mater.* **2009**, *21*, 3823.
(44) Innocenzi, P.; Falcaro, P.; Grosso, D.; Babonneau, F. *J. Phys. Chem. B* **2003**, *107*, 4711.
(45) Socrates, G. *Infrared and Raman Characteristic Group Frequencies: Tables and Charts*, 3rd ed.; John Wiley & Sons Ltd.: Chichester, U.K., 2004.
(46) Fang, J.; Wang, H.; Xue, Y.; Wang, X.; Lin, T. *ACS Appl. Mater. Interfaces* **2010**, *2*, 1449.
(47) Vilčnik, A.; Jerman, I.; Vuk, A. Š.; Koželj, M.; Orel, B.; Tomšič, B.; Simončič, B.; Kovač, J. *Langmuir* **2009**, *25*, 5869 and ref 27 cited therein.
(48) Pretsch, E.; Bühlmann, P.; Badertscher, M. *Structure Determination of Organic Compounds—Tables of Spectral Data*, 4th ed.; Springer-Verlag: Berlin, Germany, 2009.
(49) Kumar, R.; Chen, H.-T.; Escoto, J. L. V.; Lin, V. S.-Y.; Pruski, M. *Chem. Mater.* **2006**, *18*, 4319.
(50) Kecht, J.; Bein, T. *Microporous Mesoporous Mater.* **2008**, *116*, 123.
(51) Moulder, J. F.; Stickle, W. F.; Sobol, P. E.; Bomben, K. D. *Handbook of X-ray Photoelectron Spectroscopy*; Chastain, J., King, R. C., Jr., Eds.; Physical Electronics, Inc.: Eden Prairie, MN, 1995.
(52) Hozumi, A.; Ushiyama, K.; Sugimura, H.; Takai, O. *Langmuir* **1999**, *15*, 7600.
(53) Samir, O. M.; Somashekar, R. *Bull. Mater. Sci.* **2007**, *30*, 503.
(54) Li, F.; Xing, Y.; Ding, X. *Surf. Coat. Technol.* **2008**, *202*, 4721.
(55) Pereira, C.; Pereira, A. M.; Quaresma, P.; Tavares, P. B.; Pereira, E.; Araújo, J. P.; Freire, C. *Dalton Trans.* **2010**, *39*, 2842.
(56) Chung, C.; Lee, M.; Choe, E. K. *Carbohyd. Polym.* **2004**, *58*, 417.